Wave-equation migration velocity analysis with extended common-image-point gathers

Tongning Yang and Paul Sava, Center for Wave Phenomena, Colorado School of Mines

SUMMARY

Wave-equation migration velocity analysis (WEMVA) is an image-domain velocity model building technique based on band-limited wave propagation and designed especially for complex subsurface environments. It exploits the coherency of reflection events measured in extended images produced by a cross-correlation imaging condition with non-zero lags. Conventional approaches use either space-lags or time-lag common image gathers, in which only partial information of the extended images is used for velocity updates. We propose an WEMVA approach using the complete information from both space-lags and time-lags of extended images. With this approach, the velocity model building benefits both from the robustness of using the time-lag information and from the high resolution of using the space-lags information. Such an implementation is facilitated by using extended common-image-point gathers (CIPs) constructed sparsely along reflections and defined jointly for space- and time-lags. These CIPs avoid the bias towards nearly-horizontal reflectors so that steeply dipping events are well preserved in the gathers and the corresponding information related to velocity can be used. Also, the computation of the extended images can be avoided in areas where the velocity is known, e.g., inside salt bodies, or areas where the signal-to-noise ratio is too low, e.g., in shadow zones. Using CIPs for WEMVA can reduce the cost of constructing extended images and offer flexibility for the velocity model building.

INTRODUCTION

For seismic exploration in regions characterized by complex subsurface structure, wavefield-based migration is a powerful tool for accurately imaging the earth's interior that has become a commercial routine. However, since wavefield-based migration is sensitive to velocity error, the quality of the final image greatly depends on the accuracy of the velocity model. Thus, a key challenge for imaging in complex geology is an accurate determination of the velocity model in the area under investigation.

In practice, all velocity model building techniques require an information carrier to connect the input (the quantity we can measure from the data), to the output (the unknown quantity we want to resolve). Ray-based methods are techniques which use high-frequency asymptotic rays as the information carrier (Bishop et al., 1985; Stork, 1992; Liu, 1997); while wavefield-based methods are techniques which use band-limited wavefields as the information carrier (Tarantola, 1984; Pratt, 1999; Sava and Biondi, 2004; Operto et al., 2007; Shen and Symes, 2008).

In complex geology, a wavefield-based velocity analysis technique is expected to provide a more accurate, robust and consistent solution because of its accurate description of wave propagation in a complex subsurface, capability of handling strong velocity variation, and a frequency band that is consistent with wavefield-based migration. As a result, wavefield-based methods are appropriate for building a velocity model in complex geologic areas. However, the expensive computational cost, reliance on the starting model, and convergence of the results at local minimum are all issues that need to be solved for practical application of wavefield-based methods (Etgen et al., 2009; Virieux and Operto, 2009).

Wavefield-based velocity analysis techniques can be classified by the domain in which the optimization problem is formulated. In the data domain, wavefield-based velocity estimation techniques are described as full- waveform inversion (FWI) (Tarantola, 1987; Mora, 1988; Song et al., 1995), while they are referred to as wavefield-based MVA when implemented in the image domain (Biondi and Sava, 1999; Shen et al., 2003; Albertin et al., 2006; Shen and Symes, 2008; Symes, 2008). The essential difference between these two categories is that FWI defines residuals by directly measuring the misfit between observed and predicted data, while WEMVA defines residuals by measuring the coherency and focusing of extended images.

Earlier research on image-domain wavefield tomography uses space-lag common-image-gathers (CIGs), which include only partial information of migrated images (Sava and Biondi, 2004; Shen and Symes, 2008). The additional information embedded in time-lag CIGs, however, has yet to be fully exploited (Yang and Sava, 2009). An approach that simultaneously uses all lags information from the images can benefit from the high resolution of space-lag gathers and the robustness of time-lag gathers, thus having the potential to render an accurate and high-resolution velocity model in complex geology.

In this paper, we introduce an WEMVA approach based on images with complete space- and time-lag extensions. We illustrate the operators necessary for the construction of the approach, which include the migration with the extended images, forward and scattering operators with extended images. Also, we demonstrate the characteristics of the operators with the Sigsbee 2A model.

MIGRATION WITH EXTENDED IMAGES

Under the assumption of single scattering at discontinuities in the subsurface, we can describe seismic migration

as a two-steps imaging process: wavefield reconstruction followed by the application of an imaging condition.

Seismic waves generated from the source, represented by the source wavefield, propagate in the medium and interact with discontinuities. The reflected seismic waves, represented by the receiver wavefield, propagate back to the surface and are recorded by geophones. These two wavefields kinematically coincide at discontinuities. Therefore, after we reconstruct the wavefields by solving a wave equation numerically, we can extract the reflectivity information from the reconstructed wavefields using a conventional imaging condition (Claerbout, 1985),

$$R(\mathbf{x}) = \sum_{\omega} \overline{W_s(\mathbf{x},\omega)} W_r(\mathbf{x},\omega) \ , \tag{1}$$

or an extended imaging condition,

$$R(\mathbf{x},\boldsymbol{\lambda},\tau) = \sum_{\omega} \overline{W_s(\mathbf{x}-\boldsymbol{\lambda},\omega)} W_r(\mathbf{x}+\boldsymbol{\lambda},\omega)\, e^{2i\omega\tau} \ . \tag{2}$$

The image R is a function of space coordinates $\mathbf{x}$, of the space-lag $\boldsymbol{\lambda}$ and time-lag extensions τ (Rickett and Sava, 2002; Sava and Fomel, 2006; Sava and Vasconcelos, 2009). The complete set of extended images is a multi-dimensional hypercube, which allows us to simultaneously access the semblance and focusing information about the images.

Seismic modeling is a process which maps the reflectivity of the subsurface into data D recorded on the surface can be formulated using a linear operator $\mathbf{L}$ applied to the reflectivity model represented by the image R:

$$D = \mathbf{L}R \ . \tag{3}$$

Since the modeling is a linear process, the adjoint process can be directly obtained. Such an adjoint process is referred to as migration, and can be conceptually formulated as applying the operator $\mathbf{L}^*$ to data D and to obtain the image R. If we use matrix notation, we have

$$R = \mathbf{L}^* D \ . \tag{4}$$

MIGRATION VELOCITY ANALYSIS WITH EXTENDED IMAGES

To formulate the velocity analysis in the image-domain, we first need to construct an objective function for the optimization problem. In general, there are two approaches we can use to seek the solution. The first approach uses a linearized image perturbation and the second approach is based on differential semblance optimization. Here we concentrate on the first approach. To obtain an image perturbation, one starts by applying a Taylor expansion to an image as follows:

$$R(\mathbf{x},s_c) = R(\mathbf{x},s_b) + \Delta R(\mathbf{x}) \ , \tag{5}$$

where

$$s_c = s_b + \Delta s \ . \tag{6}$$

Here, s_c denotes the correct slowness and s_b and Δs denote background slowness and slowness perturbation, respectively. The image perturbation is related to the slowness perturbation by a linearized scattering operator $\mathbf{A}$:

$$\Delta R(\mathbf{x}) = \mathbf{A}\Delta s(\mathbf{x}) \equiv \frac{\partial R(\mathbf{x},s)}{\partial s}|_{s=s_b} \Delta s(\mathbf{x}) \ . \tag{7}$$

Since the image perturbation is proportional to the slowness perturbation, the velocity analysis can be performed by minimizing the image perturbation. Thus, the corresponding objective function, which defines a linearized optimization problem, is formulated as:

$$J(\Delta s) = \frac{1}{2}\|\Delta R - \mathbf{A}\Delta s\|_2^2 \ . \tag{8}$$

The operator $\mathbf{A}$ in equations 7 and 8 is used to obtain an image perturbation from a slowness perturbation:

$$\Delta R = \mathbf{A}\Delta s \ . \tag{9}$$

We can directly construct the adjoint MVA process similarly to migration. In this way, we obtain the adjoint pair of operators. The adjoint process describes the backprojection from image perturbation to slowness perturbation:

$$\Delta s = \mathbf{A}^* \Delta R \ , \tag{10}$$

where $\mathbf{A}^*$ represents the adjoint operator.

We use the Sigsbee 2A dataset (Paffenholz et al., 2002) as an example with the background model in Figure 1(a) and with the slowness perturbation in Figure 1(b). We first create the image perturbation using the forward MVA process given by equation 9. We construct the image perturbation for CIPs located at the positions indicated by dots in Figure 1(c). Some CIPs at the locations indicated by the symbol $*$ are shown in Figures 2(a)-2(d).

For all CIPs shown here, the events exhibit residual moveout in the λ_x-τ panels. According to Sava and Vasconcelos (2009), the kinematics of the extended images when the velocity used for imaging is correct are given by

$$R(\boldsymbol{\lambda},\tau) = \delta(\mathbf{q}\cdot\boldsymbol{\lambda})\,\delta(v\tau) \ , \tag{11}$$

where $\mathbf{q}$ denotes a unit vector parallel to the reflector and at the intersection of the reflection and reflector planes, and δ is the Kronecker symbol. Since we use an incorrect background velocity model, the residual moveout is the image imperfection and indicates velocity errors. In addition, in Figures 2(c), the CIPs are constructed in the subsalt area with an uneven illumination. The salt creates uneven illumination and shadow zones, which generate artifacts and distort the images. The distortion is similar to the imperfections caused by the velocity error. If we use such gathers for velocity analysis, we may obtain an incorrect result. Thus, in complex area, illumination compensation is necessary for velocity model building. This important research direction falls outside the scope of this paper.

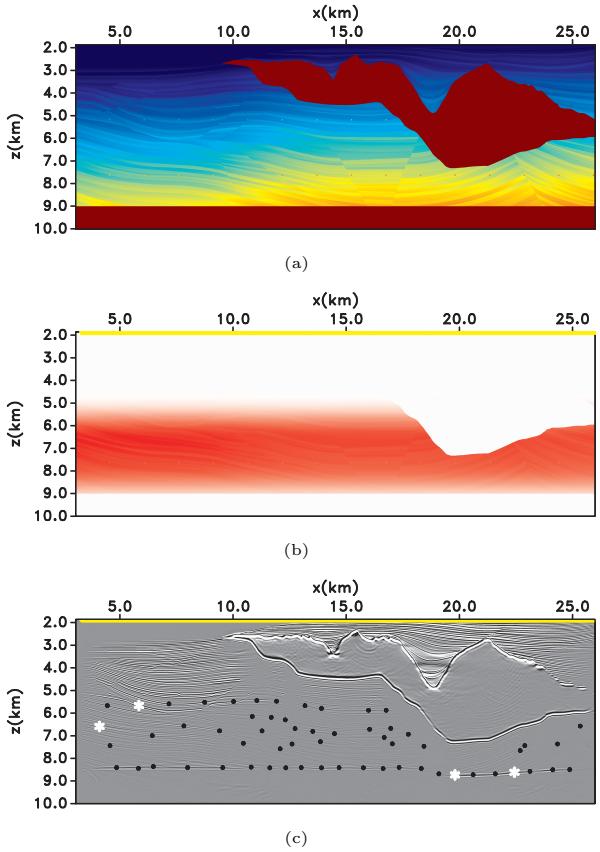

Figure 1: (a) Sigsbee 2A synthetic model, (b) slowness perturbation and (c) migrated image with background velocity model. The dots indicate the positions where CIPs are constructed. The $*$ indicate the positions of the CIPs shown in Figures 2.

Next, we apply the adjoint MVA process given by equation 10 to the image perturbation to obtain the backprojection, which is equivalent to the gradient of the corresponding objective function given by equation 8. The backprojection provides a straightforward way to study the forward and adjoint scattering operators. The main factors that control the shape of the backprojection are (1) the frequency content of the background wavefields, (2) the type of source (e.g., point or plane-wave) from which we generate the background wavefields, and (3) the type of perturbation constructed in the image space. Figure 3(a)-3(b) show the backprojection from a single shot at $x = 12.3$ km using different frequency bands. We can observe how the kinematics of the backprojection change with the frequency band. With increasing number of frequencies used in the process, the magnitude of the backprojection become stronger. Figure 3(c)-3(d) show the backprojection from all shots using different frequency bands. Similarly, the magnitude of the backprojection is increasing with more frequencies used. In Figure 3(d), the shape of the salt is clearly visible in the backprojection since we limit the slowness perturbation only in the subsalt area and the background velocity model contains the correct information about the salt. Thus, the complicated pattern of the backprojection is due to the complexity of the background model. Also, we notice that the backprojected slowness is unevenly distributed in the model. The main reason is that the left area is well-illuminated, which leads to a larger contribution to the backprojection from the CIPs in left area than from the CIPs in the subsalt area. Iterative inversion using the operators described earlier re-balances the anomaly magnitude throughout the model.

In practice, the true slowness perturbation is never known, so the image perturbation is also unknown. However, one can construct a linearized image perturbation to approximate the true one. Thus, the key element for this approach is the construction of the linearized image perturbation. Sava (2003) proposes using Stolt residual migration as the solution, while Yang and Sava (2009) use focusing of the time-lag extended images to address the problem. Generally, the linearized-image perturbation approach can effectively avoid the common cycle-skipping problem for wavefield tomography. The construction of the linearized image perturbation, however, requires a quantity that can be measured directly from the image. Such a quantity is difficult to measure for all types of extended images. How to construct a linearized image perturbation for CIPs remains object of future research.

CONCLUSIONS

We discuss image-domain wavefield-based migration velocity analysis using extended images analyzed in common-image-point gathers constructed at sparse locations in the image. We introduce the key elements for the implementation, which are the migration, forward and adjoint linearized scattering operators with extended images. These operators are necessary components for the velocity updating procedure. Synthetic examples demonstrate the feasibility of using common-image-point gathers for velocity model building in complex geologic regions. The implementation of WEMVA with extended images can be done cheaply by using a sparse distribution of points in the subsurface and by using narrow frequency bands in backprojections.

ACKNOWLEDGMENTS

This work is supported in part by the sponsors of the Center for Wave Phenomena at Colorado School of Mines and by a research grant from Statoil. We thank Thomas Cullison for support with CIPs location used in the examples. The reproducible numeric examples in this paper use the Madagascar open-source software package freely available from
http://www.reproducibility.org.

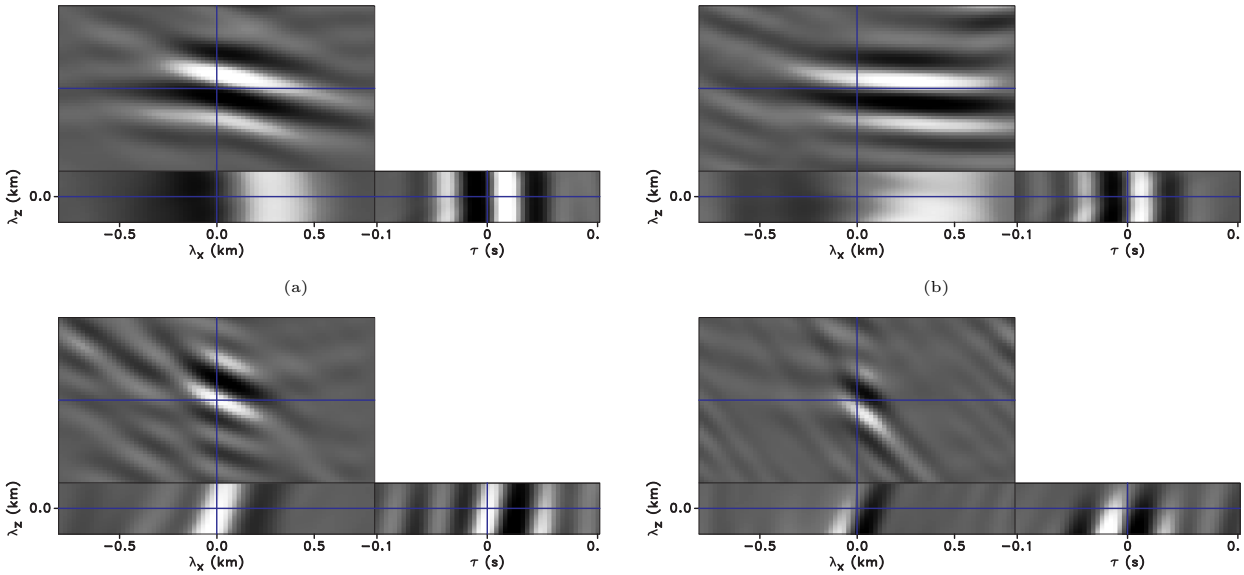

Figure 2: Image perturbation of CIPs chosen at (a) $x = 4.1$ km, $z = 6.6$ km (b) $x = 5.8$ km, $z = 5.7$ km, (c) $x = 19.8$ km, $z = 8.7$ km, and (d) $x = 22.4$ km, $z = 8.6$ km.

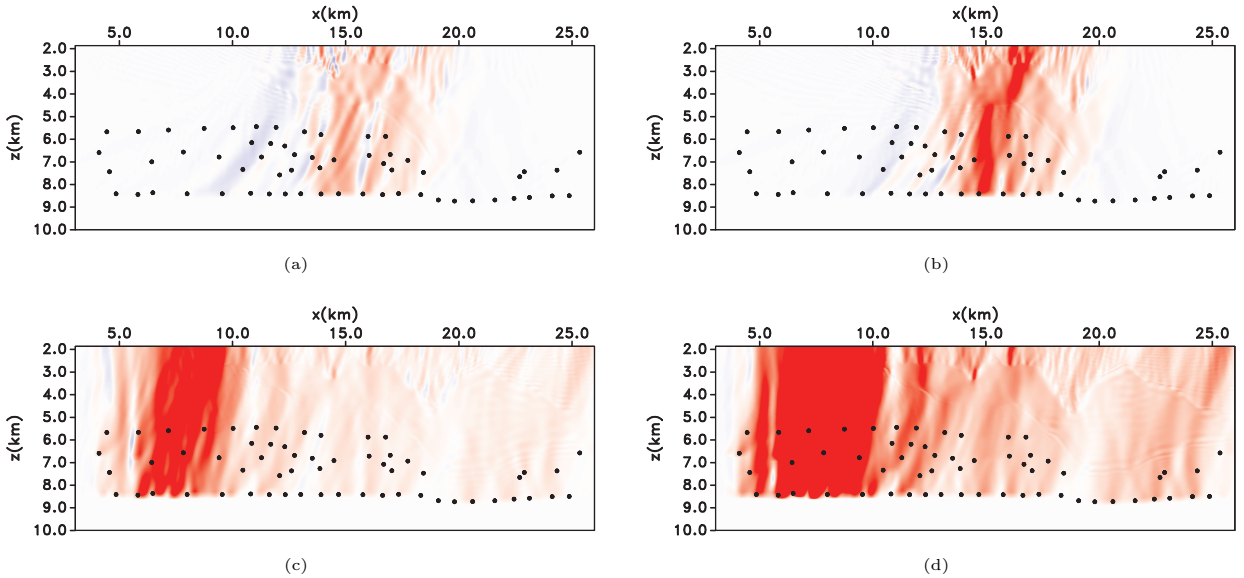

Figure 3: Backprojection from the image perturbation of all CIPs (a) using a frequency band from 3-4.5 Hz and a single shot at $x = 12.3$ km, (b) using a frequency band from 3-8.5 Hz and a single shot at $x = 12.3$ km, (c) using a frequency band from 3-4.5 Hz and all shots, (d) using a frequency band from 3-8.5 Hz and all shots.